

Approximate Bayesian Kernel Machine Regression via Random Fourier Features for Estimating Joint Health Effects of Multiple Exposures

Danlu Zhang^{1,*}, Stephanie M. Eick², and Howard H. Chang^{1,2}

¹ Department of Biostatistics and Bioinformatics, Emory University,
Atlanta, Georgia, USA

² Gangarosa Department of Environmental Health, Emory University,
Atlanta, Georgia, USA

* danlu.zhang@emory.edu

Abstract

Environmental epidemiology has traditionally focused on examining health effects of single exposures, more recently with adjustment for co-occurring exposures. Advancements in exposure assessments and statistical tools have enabled a shift towards studying multiple exposures and their combined health impacts. Bayesian Kernel Machine Regression (BKMR) is a popular approach to flexibly estimate the joint and nonlinear effects of multiple exposures. However, BKMR faces computation challenges for large datasets, as inverting the kernel repeatedly in Markov chain Monte Carlo (MCMC) algorithms can be time-consuming and often infeasible in practice. To address this issue, we propose a faster version of BKMR using supervised random Fourier features to approximate the Gaussian process. We use periodic functions as basis functions and this approximation re-frames the kernel machine regression into a linear

mixed-effect model that facilitates computationally efficient estimation and prediction. Bayesian inference was conducted using MCMC with Hamiltonian Monte Carlo algorithms. Analytic code for implementing Fast BKMR was developed for R. Simulation studies demonstrated that this approximation method yields results comparable to the original Gaussian process while reducing the computation time by 29 to 99%, depending on the number of basis functions and sample sizes. Our approach is also more robust to kernel misspecification in some scenarios. Finally, we applied this approach to analyze over 270,000 birth records, examining associations between multiple ambient air pollutants and birthweight in Georgia.

Keywords: Bayesian Kernel Machine Regression; random Fourier features; multiple exposures.

1 Introduction

Most environmental epidemiological studies focus on estimating the health effects of a single exposure one-at-a-time, sometimes adjusting for other exposures. However, humans are exposed to multiple environmental risk factors simultaneously and the majority of exposures are correlated due to common sources or exposure pathways (Billionnet et al., 2012). Recent and continual developments of statistical approaches have facilitated our ability to examine joint effects of multiple exposures (Sexton, 2012; Benka-Coker et al., 2020). For example, previous studies have documented joint effects of multiple air pollutants on adverse health outcomes, such as bladder cancer incidence (Kim et al., 2024), childhood persistent asthma (Shiroshita et al., 2024) and low birthweight (Yang et al., 2020).

Bayesian kernel machine regression (BKMR) is one widely used method to estimate joint effects of multiple exposures (Bobb et al., 2014). Compared to other commonly used models, such as weighted quantile sum regression (WQS) and quantile g-computation (qgcomp), BKMR assumes that the complex nonlinear exposure-response surface is a random realization of a Gaussian process specified by its kernel function (Bobb et al., 2014). Hence,

one can easily derive marginal effect of any exposure combination, offering a flexible way to evaluate health effects without pre-specifying exposure contrasts of interest (Bobb et al., 2014; Li et al., 2022). BKMR has also been shown to provide reliable inference in complex and high-dimensional exposure settings.

Kernel regression models are known to be computationally intensive due to the need to invert the $n \times n$ kernel matrix, where n is the sample size. This issue is exacerbated in BKMR due to its use of Markov Chain Monte Carlo (MCMC) for posterior inference. Currently, BKMR can be impractical for moderately large datasets (e.g. with sample sizes around 5,000) and as a result, BKMR is more commonly used in analyzing health effects of chemical exposures from cohort studies with a relatively small sample size (Zhuang et al., 2021; Eick et al., 2024; Preston et al., 2020), rather than with large administrative health databases where sample sizes are often in the tens of thousands or larger. Current implementation of BKMR offers an option to use predictive process where exposures are projected to a lower dimensional space spanned by the set of knots. (Bobb et al., 2018; Banerjee et al., 2008). However, this approach has been noted for challenges with overs-smoothing (Banerjee, 2017; Finley et al., 2009), and there has been little guidance on knot selection in multivariate Gaussian process settings. One possibility is to use a grid of exposure quantiles as knots (e.g., all combinations of exposure deciles), but the number of knots increases quickly as the number of exposures included in the exposure matrix increases. We are not aware of BKMR with predictive process being used in practice.

One common way to reduce the memory requirement and computational cost is with low-rank approximation, which is widely used in large-scale data applications (Kishore Kumar and Schneider, 2017). According to the spectral representation theorem, trigonometric functions can be used as basis functions to capture essential characteristics of the data with fewer parameters (Miller and Reich, 2022). Random Fourier features (RFF) with frequencies sampled from a known spectral density can be used to approximate Gaussian process in a kernel machine setting. (Rahimi and Recht, 2007). This allows for the application of

kernel methods with linear algorithms, significantly improving scalability while maintaining approximation quality. Although the original RFF is a data-independent approach, it has been extended to be data-driven (supervised) in several ways for large real-world applications (Liu et al., 2021; Chang et al., 2017). RFF has also recently been examined for analyzing large spatial dataset (Miller and Reich, 2022).

The main objective of this paper is to adopt and evaluate the use of RFF as a low-rank approximation method to BKMR in order to reduce the computation time. We chose this low-rank method because this approximation re-frames the kernel machine regression into a linear mixed-effect model that facilitates computationally efficient estimation and prediction under a Bayesian framework. The rest of the paper is organized as follows. In Section 2, we introduce the proposed method, which we call Fast BKMR. In Section 3, we present simulation studies and compare our results with the original BKMR when possible under different settings. In Section 4, we apply Fast BKMR to characterize associations between birthweight and multiple ambient air pollutions to highlight the ability of Fast BKMR to handle a large sample size and to capture complex exposure-response functions. In Section 5, we discuss the advantages and limitations of this approximation method and potential further extensions.

2 Methods

2.1 Bayesian Kernel Machine Regression for Multiple Exposures

We first describe the current formulation of BKMR for multiple exposures (Bobb et al., 2014). For individual $i = 1, \dots, n$, let y_i denote the outcome of interest and $\mathbf{x}_i = (x_{1,i}, \dots, x_{M,i})$ denote the vector of M exposures. We assume the following linear regression model

$$y_i = h(\mathbf{x}_i) + \mathbf{Z}_i^T \boldsymbol{\gamma} + \epsilon_i \tag{1}$$

where $h(\mathbf{x}_i)$ is the individual-specific association between \mathbf{x}_i and the outcome, \mathbf{Z}_i is the vector of confounders with corresponding regression coefficient $\boldsymbol{\gamma}$, and $\epsilon_i \sim N(0, \sigma^2)$ is the residual error. BKMR represents $h(\mathbf{x})$ non-parametrically as a realization from a Gaussian process, characterized by the kernel

$$\mathcal{K}(\mathbf{x}_i, \mathbf{x}_j) = \exp\left(-\sum_{m=1}^M \theta_m (x_{m,i} - x_{m,j})^2\right) \quad (2)$$

Hence, effects of multiple exposures are more similar for individuals with smaller squared Euclidean distance between exposure levels. The above kernel also assumes separability between exposures, such that the correlation decreases multiplicatively by exposures and the importance of each exposure is allowed to vary via the exposure-specific parameter $\theta_m \geq 0$.

The joint distribution of $\mathbf{h} = [h(\mathbf{x}_1), \dots, h(\mathbf{x}_n)]^T$ is multivariate Normal with covariance matrix $\tau^2 \mathbf{K}$, where τ^2 is the marginal variance and \mathbf{K} is an $n \times n$ matrix with entries given by the kernel function. Bayesian inference via MCMC can be computationally challenging for large sample size n due to the need to repeatedly evaluate \mathbf{K}^{-1} .

2.2 Kernel Approximation by Random Fourier Features

Bochner's theorem (Rudin, 2017) states that any positive definite and stationary kernel can be expressed as the Fourier transform of its spectral density $f(\boldsymbol{\omega})$:

$$\mathcal{K}(\mathbf{x}_i - \mathbf{x}_j) = \int \exp\{i\boldsymbol{\omega}^T(\mathbf{x}_i - \mathbf{x}_j)\} f(\boldsymbol{\omega}) d\boldsymbol{\omega} \quad (3)$$

where $\boldsymbol{\omega} \in \mathbb{R}^M$ is the frequency and $i = \sqrt{-1}$. Consequently, the random effect $h(\mathbf{x}_i)$ can be rewritten as

$$h(\mathbf{x}_i) = \int \exp(i\boldsymbol{\omega}^T \mathbf{x}_i) [a(\boldsymbol{\omega}) + ib(\boldsymbol{\omega})] d\boldsymbol{\omega} \quad (4)$$

where $a(\boldsymbol{\omega})$ and $b(\boldsymbol{\omega})$ are mean-zero random variables that are independent between $\boldsymbol{\omega}$ and have $\text{Var}[a(\boldsymbol{\omega}) + ib(\boldsymbol{\omega})] = \tau^2 f(\boldsymbol{\omega})$. Since $h(\mathbf{x}_i)$ is real-valued, the integral can be approxi-

mated by finite set of frequencies $\{\boldsymbol{\omega}_1, \dots, \boldsymbol{\omega}_J\}$,

$$h(\mathbf{x}_i) = \sum_{j=1}^J a_j \cos(\boldsymbol{\omega}_j^T \mathbf{x}_i) + b_j \sin(\boldsymbol{\omega}_j^T \mathbf{x}_i) \quad (5)$$

Equation (5) can be viewed as a set of basis expansions using periodic functions with amplitudes a_j and b_j as random-effect coefficients to be estimated from the data. For the Gaussian process and kernel function specified by BKMR, these correspond to

$$\boldsymbol{\omega}_j \sim N(\mathbf{0}, \Sigma) \quad \text{and} \quad a_j, b_j \sim N(0, \tau^2/J)$$

where Σ is an $m \times m$ diagonal matrix with elements $\{2\theta_1, \dots, 2\theta_M\}$. This approximation re-frames the kernel machine regression into a linear mixed-effect model that facilitates computationally efficient parameter estimation and prediction. It can be shown that marginalizing over a_j and b_j , the induced $\text{Cov}\{h(\mathbf{x}_i), h(\mathbf{x}_j)\}$ has expectation $\mathcal{K}(\mathbf{x}_i, \mathbf{x}_j)$ and the variance decreases as a function of J . Moreover, by treating the frequency $\boldsymbol{\omega}_j$ as a random variable, we can learn the optimal finite number of frequencies to use from the data.

We complete the Bayesian hierarchical model specification by assigning improper flat prior for the regression coefficients $\boldsymbol{\gamma}$ with $N(0, \sigma_\gamma^2 \mathbf{I})$, inverse-Gamma distributions for the residual variance $\sigma^2 \sim \text{IG}(0.001, 0.001)$, the Gaussian process marginal variance $\tau^2 \sim \text{IG}(0.001, 0.001)$, and $\theta_1, \dots, \theta_M \sim \text{IG}(0.001, 0.001)$.

2.3 Bayesian Inference and Estimation

Hamiltonian Monte Carlo (HMC; (Neal, 2011)) is an approach to generate posterior samples in high-dimensional space which is suitable to deal with the label-switching problem in Bayesian analysis (Miller and Reich, 2022). We implement HMC using a leapfrog integrator. Let \mathcal{L} , e , and L denote the log-density, step-size parameter and number of steps, respectively. Starting at the initial location θ^0 , the idea of HMC at m^{th} iteration is as follows.

Step 1: Sample r^0 from $N(0, I)$ and set $\theta^m \leftarrow \theta^{m-1}$, $\tilde{\theta} \leftarrow \theta^{m-1}$ and $\tilde{r} \leftarrow r^0$.

Step 2: for $l = 1, \dots, L$, set $\tilde{\theta}, \tilde{r} \leftarrow \text{Leapfrog}(\tilde{\theta}, \tilde{r}, e)$.

Step 3: Update θ^m and r^m by $\tilde{\theta}$ and $-\tilde{r}$ with probability $\alpha = \min\{1, \frac{\exp(\mathcal{L}(\tilde{\theta}) - \frac{1}{2}\tilde{r} \cdot \tilde{r})}{\exp(\mathcal{L}(\theta^{m-1}) - \frac{1}{2}r^0 \cdot r^0)}\}$.

To tune e to achieve the acceptance rate of 65 – 85%, we checked the acceptance rate per 200 iterations in burn-in samples. If the acceptance rate is over 85%, e will be replaced by $e(1 + e_t)$, where $e_t \in [0, 1]$ is the tuning rate. In contrast, if the acceptance rate is lower than 65%, e will be set to $e(1 - e_t)$. The Leapfrog(θ, r, e) is defined as:

Step 1: Set $\tilde{r} \leftarrow r + (e/2)\nabla_{\theta}\mathcal{L}(\theta)$.

Step 2: Set $\tilde{\theta} \leftarrow \theta + e\tilde{r}$.

Step 3: Set $\tilde{r} \leftarrow \tilde{r} + (e/2)\nabla_{\theta}\mathcal{L}(\tilde{\theta})$.

Step 4: Return $\tilde{\theta}$ and \tilde{r} .

Bayesian inference is conducted by posterior sampling using Markov chain Monte Carlo (MCMC). We first initialize $\theta_1, \dots, \theta_M$ and then simulate $\omega_1, \dots, \omega_J$ from $N(0, \Sigma)$. Basis functions are constructed via $\cos(\omega_j^T x_i)$ and $\sin(\omega_j^T x_i)$, $j = 1, \dots, J, i = 1, \dots, n$. Next, we utilize penalized regression to estimate a_j, b_j and γ . Last step in initialization is to estimate τ^2 and σ^2 . In MCMC iteration, Gibbs updates are used for σ^2, τ^2 and $\theta_1, \dots, \theta_M$. $(\gamma, a_1, \dots, a_J, b_1, \dots, b_J)$ are updated via HMC as one block and $\omega_1, \dots, \omega_J$ are also updated via HMC as another block. Log-likelihoods and first derivatives of log-likelihood used in the HMC updates can be found in Web Appendix A.

Watanabe-Akaike Information Criterion (WAIC) can be used to select the number of basis functions J . WAIC is helpful for models with hierarchical structures. WAIC is defined as $-2(\text{lppd} - p_{\text{WAIC}})$, where lppd is the sum of log point-wise predictive densities and p_{WAIC} denotes the sum of posterior variance of the log predictive density for each data point y_i (Gelman et al., 2013). We discarded the first half of Markov chain Monte Carlo samples,

Algorithm 1 MCMC iterations of Fast BKMR

Input: Data: $\{y_i, \mathbf{x}_i, \mathbf{z}_i\}_{i=1}^n$, e_β , e_ω , J , σ_γ^2 , $(\theta_1, \dots, \theta_M)$, τ^2 , σ^2 .

Initialization:

Simulate $\boldsymbol{\omega}_j^0 \sim N(\mathbf{0}, \Sigma)$, $j = 1, \dots, J$ where $\Sigma = \text{diag}(2\theta_1, \dots, 2\theta_M)$.

Construct basis functions $\cos(\boldsymbol{\omega}_j^{0T} \mathbf{x}_i)$ and $\sin(\boldsymbol{\omega}_j^{0T} \mathbf{x}_i)$.

Estimate a_j^0 , b_j^0 and $\boldsymbol{\gamma}^0$ via penalized regression using σ_γ^2 , τ^2 , σ^2 and input data.

Estimate σ_0^2 .

for k in $1, \dots, K$ **do**

Update $\theta_1^k, \dots, \theta_M^k$ via Inverse Gamma $(0.001 + \frac{J}{2}, 0.001 + \frac{1}{2} \sum_{j=1}^J \boldsymbol{\omega}_j^{(k-1)T} \boldsymbol{\omega}_j^{(k-1)})$.

Update $(\boldsymbol{\gamma}^k, a_1^k, \dots, a_J^k, b_1^k, \dots, b_J^k)$ as a block via HMC.

Update $\boldsymbol{\omega}_1^k, \dots, \boldsymbol{\omega}_J^k$ as a block via HMC.

Update τ_k^2/J via Inverse Gamma $(0.001 + J, 0.001 + \frac{1}{2} \sum_{j=1}^J (a_j^k)^2 + (b_j^k)^2)$.

Update σ_k^2 via Inverse Gamma $(0.001 + \frac{n}{2}, 0.001 + \frac{1}{2} \sum_{i=1}^n (y_i - \hat{y}_i^k)^2)$.

Calculate $h(\mathbf{x}_i^k)$ via $\sum_{j=1}^J a_j^k \cos(\boldsymbol{\omega}_j^{kT} \mathbf{x}_i) + b_j^k \sin(\boldsymbol{\omega}_j^{kT} \mathbf{x}_i)$.

end for

and inference was conducted using the second half of posterior samples. All computations were conducted in R version 4.2.2 (R Core Team, 2022) and the R package, `bkmr` version 0.2.2, was used to utilize the original BKMR (Bobb, 2022). We also provide example R code for implementing Fast BKMR in Web Appendix B.

3 Simulation Studies

3.1 Setup

We generated datasets of N observations $\{y_i, \mathbf{x}_i, \mathbf{z}_i\}_{i=1}^N$, where $\mathbf{x}_i = (x_{i1}, \dots, x_{iM})^T$ represents an exposure profile with M exposures and $\mathbf{z}_i = (z_{i1}, \dots, z_{iP})^T$ denotes P confounders for individual i . We examined 2, 5 and 10 exposures and all exposures were simulated from Normal distributions with mean zeros and different variances. Five confounders were generated from either the Normal distribution or Binomial distributions. $h(\mathbf{x}_i)$ was simulated from a Gaussian process with kernel \mathbf{K} with different levels of correlation: strong (correlations between 0.75 and 0.9) and weak (correlations between 0.1 and 0.3). Outcome y_i was simulated from $N(h(\mathbf{x}_i) + \mathbf{z}_i^T \boldsymbol{\gamma}, \sigma^2)$. We also examined scenarios where BKMR incor-

rectly specifies the kernel, with the true kernel being either $\exp(-\sum_{m=1}^M \theta_m \sqrt{|x_{im} - x_{jm}|})$ or $\exp(-\sum_{m=1}^M \theta_m |x_{im} - x_{jm}|)$. We tested both original BKMR and Fast BKMR with sample sizes N of 200 and 500 across 100 simulations. Since the BKMR R package is not computationally practical with 1000 observations across 100 simulations, we examined the original BKMR only across 40 simulations with 1000 observations.

Within each simulated dataset, different number of basis functions ($J = 5, 20, 50, 100,$ and 200) were examined to identify the most appropriate J based on WAIC. We used the estimated $\theta_m, m = 1, \dots, M$ obtained from BKMR R package using a sub-sample of 100 observations as the initial values for θ_m in the Fast BKMR method. Model performance was evaluated by comparing the root mean squared error (RMSE) between the estimated $\hat{h}(\mathbf{x}_i)$ and the true $h(\mathbf{x}_i)$.

We also evaluated the model’s ability to perform out-of-sample prediction. We generated 20%, 30%, 40% and 50% more data and left those out as testing data. The RMSE between the estimated exposure-response function $\tilde{h}(\mathbf{x}_i^{new})$, using exposure values in testing data, and the true $h(\mathbf{x}_i)$ was calculated to evaluate model’s ability.

3.2 Results

Simulation results of RMSE for in-sample tests are presented in Figure 1. Across the different sample sizes, the original BKMR showed a lower RMSE compared to our approximation method with the weak correlation between exposures; however, Fast BKMR performed comparable to the original BKMR when the correlation between 2 or 5 exposures is strong. When we had 10 or 5 exposures with the strong correlation, our approximation method with 5 basis functions performed even better than the original BKMR. As the number of exposures increases, the joint effects become more complex, and our approximation framework offers greater flexibility in capturing these effects. Regardless of sample size, weak correlations between exposures and a small number of basis functions are associated with larger RMSE. In contrast, when the correlation between exposures is strong, the RMSE decreases

with fewer basis functions, and this trend is especially noticeable when there are 5 or 10 exposures. For sample sizes of 500 or 1000, RMSE remains almost unchanged across different numbers of basis functions when there are only 2 exposures. Overall, lower RMSE were observed when the correlation between exposures are strong and the number of exposures is small. We observed similar patterns for out-of-sample evaluation (Web Figure 1).

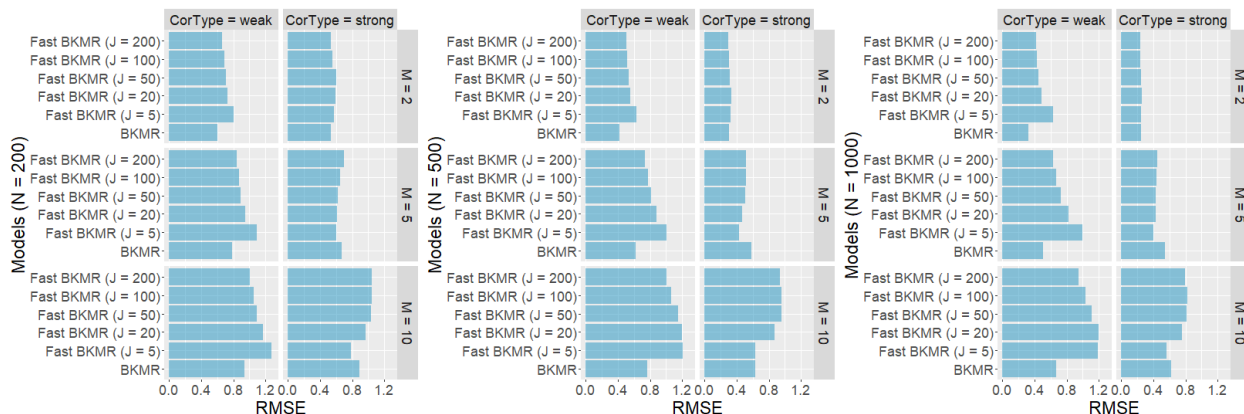


Figure 1: The RMSE between true and estimated joint effects with different correlation type (CorType), number of exposures (M) and sample size (N). RMSE for sample size at 1000 from the BKMR R package were calculated across 40 simulations.

In the presence of kernel misspecifications, both original BKMR and Fast BKMR resulted in larger RMSE values across all combinations of sample size, number of exposures and correlation types. Compared to the correct kernel specifications, smaller RMSE was associated with strong correlations, smaller number of exposures and larger sample sizes. Although original BKMR outperformed our approximation method in scenarios with weak correlations, our method yielded comparable or even better results in scenarios with strong correlations. For out-of-sample evaluation with incorrect kernel specifications, our method had a smaller RMSE in scenarios with larger number of exposures.

Fast BKMR provided considerable reduction on computation time compared to the original BKMR as shown in Table 1. With 200 observations, original BKMR took about 8 and 10 minutes for 2 and 10 exposures, respectively, while Fast BKMR only took 0.20 and 0.25 minutes for the same number of exposures with five basis functions, resulting in a 98%

Table 1: Computation time in minutes (percentages of reduction^a for original BKMR and Fast BKMR).

| Sample Size | Type | $M^b = 2$ | $M^b = 5$ | $M^b = 10$ |
|-------------------|-------------------------|-------------|-------------|-------------|
| 200 | BKMR | 8.74 (0%) | 7.62 (0%) | 10.08 (0%) |
| | Fast BKMR ($J = 5$) | 0.20 (98%) | 0.26 (97%) | 0.25 (97%) |
| | Fast BKMR ($J = 50$) | 1.05 (88%) | 1.41 (82%) | 1.52 (85%) |
| | Fast BKMR ($J = 200$) | 3.97 (55%) | 5.42 (29%) | 6.09 (40%) |
| 500 | BKMR | 126.74 (0%) | 93.05 (0%) | 126.13 (0%) |
| | Fast BKMR ($J = 5$) | 0.36 (100%) | 0.48 (99%) | 0.49 (100%) |
| | Fast BKMR ($J = 50$) | 2.59 (98%) | 3.45 (96%) | 3.66 (97%) |
| | Fast BKMR ($J = 200$) | 10.69 (92%) | 13.97 (85%) | 15.17 (88%) |
| 1000 ^c | BKMR | 864.64 (0%) | 657.31 (0%) | 933.40 (0%) |
| | Fast BKMR ($J = 5$) | 0.64 (100%) | 0.74 (100%) | 0.89 (100%) |
| | Fast BKMR ($J = 50$) | 5.01 (99%) | 5.98 (99%) | 7.26 (99%) |
| | Fast BKMR ($J = 200$) | 20.38 (98%) | 24.33 (96%) | 29.65 (97%) |

^a percentage of reduction: $1 - \frac{\text{computation time of Fast BKMR}}{\text{computation time of BKMR}}$

^b M : the number of exposures.

^c the computation time of sample size at 1000 were calculated across 40 simulations.

reduction. The computation time increased with increasing number of basis functions but even with 200 basis functions, Fast BKMR can reduce 29% to 55% computation time. For sample size at 500, Fast BKMR took less than 16 minutes to fit one model with 200 basis functions where the reduction of computation time reached over 85%. When the sample size increased to 1000, Fast BKMR can be fitted within one minute with 5 basis functions or within 30 minutes with 200 basis functions, while original BKMR took around 15 hours to fit one model. With an increasing sample size, Fast BKMR achieved a higher reduction rate, reaching over 96% with 1,000 observations. The computation time increased almost linearly with sample size and the number of basis functions, while the number of exposures had a small impact on computation time. This indicates the increased applicability of Fast BKMR in situations where the number of exposures is high.

We examined the use of WAIC to select the number of basis functions and results are shown in Web Figure 2. Small number of basis functions were needed for exposures with strong correlation. With increasing sample size and exposures numbers, more basis functions

were preferred. For incorrect specification of the kernel, similar patterns were observed. Large number of basis functions was selected with larger sample size, more exposures and weak correlation between exposures. However, less basis functions took more proportions when the kernel was misspecified. In our setting, the correct kernel induces weaker correlation compared to the assumed model, resulting in an approximation using a smaller number of basis functions. We note that the model with the lowest WAIC among those with different numbers of basis functions did not always correspond with the lowest RMSE of joint effects since WAIC is calculated based on the predictive density of y_i , which is determined by both exposures and confounders.

4 Application to the Atlanta Birthweight and Air Pollution Study

4.1 Dataset

We analyzed data from a previous study of associations between air pollution and birthweight (Strickland et al., 2019). The birth records from 20 counties in metropolitan Atlanta were obtained from the Office of Health Indicators for Planning, Georgia Department of Public Health for the period 2002 to 2006. A total of 273,711 singleton live birth with gestational weeks of 28 to 44 were included. We excluded birthweight less than 400 grams, maternal age below 16 or over 43 years of age, presence of any congenital anomaly identified on birth record and preterm birth (gestational weeks ≤ 36) with a procedure code for induction of labor. The characteristics of study population is shown in Web Table 1.

We considered three air pollutants: 1-hour maximum carbon monoxide (CO) and nitrogen dioxide (NO₂), and 24-hour average particular matter $\leq 2.5 \mu\text{m}$ in diameter (PM_{2.5}). Air pollutant concentrations were obtained by bias-correcting 12-km grid numerical simulations from the Community Multi-scale Air Quality (CMAQ) Model with ground monitor

measurements in Georgia (Friberg et al., 2016). Birth records were linked to CMAQ grid cells using maternal address at delivery at the Census tract level, and average exposures were calculated for the entire pregnancy. A summary of exposure concentrations in original scale is shown in Web Table 2. Due to the varying ranges of the pollutants, we standardized pollutant concentrations by dividing their standard deviation.

4.2 Health Models

To compare the results of Fast BKMR with other commonly used models, we also considered single- and multi-pollutant models using linear regressions. Since Fast BKMR also allows for nonlinear effects, we modeled nonlinear NO₂, CO and PM_{2.5} associations with natural cubic splines (3 degrees of freedom) in the single pollutant model, respectively. In the multi-pollutant models, we accounted for the nonlinear effects of each of the three pollutants simultaneously and included all possible combinations of pairwise interactions between NO₂, CO, and PM_{2.5}. For Fast BKMR, we used 20 basis functions for the three pollutants. All models were adjusted for maternal race/ethnicity (white/black/Asian/Hispanic), age (modeled using a natural cubic spline with 5 df), education level (less than ninth grade, 9th–12th grade, high school, college and above), married status (married or unmarried), indicator of tobacco use during the pregnancy (yes or no), indicator of alcohol use during the pregnancy (yes or no), indicator of previous birth (yes or no), indicator of gestational weeks, indicators for county of residence at delivery, Census track percent poverty levels (modeled using a natural cubic spline with 5 df) and conception date (modeled using natural cubic spline with 12 df).

4.3 Results

The overall effects of all pollutants on birthweight differences, measured in grams, were estimated for two exposure contrasts: (1) between the 75th and 25th percentiles and (2) between the 95th and 50th percentiles of all exposures (Table 2). In both single- and multi-pollutant

Table 2: Difference in average birthweight with 95% confidence/posterior intervals (CI/PI) from single, multi-pollutant models and Fast BKMR. Effect sizes are evaluated with two different exposure contrasts with all exposures set at (1) the 75th versus the 25th percentile and (2) the 95th versus the 50th percentile.

| Model | Pollutant | 75th vs 25th (95% CI/PI) | 95th vs 50th (95% CI/PI) |
|------------------|---|---|---|
| Single pollutant | ns(NO ₂ , 3) | -16.54 (-23.93, -9.14) | -9.41 (-16.88, -1.93) |
| | ns(CO, 3) | -12.05 (-18.63, -5.48) | -7.52 (-14.05, -0.99) |
| | ns(PM _{2.5} , 3) | -5.97 (-10.26, -1.68) | -3.09 (-8.12, 1.94) |
| Multi-pollutant | ns(NO ₂ , 3) + ns(CO, 3) | -24.43 (-33.49, -15.36) | -9.99 (-19.13, -0.84) |
| | + ns(PM _{2.5} , 3) | | |
| | ns(NO ₂ , 3) + ns(CO, 3) + ns(PM _{2.5} , 3) + three pairwise interactions | -25.06 (-34.21, -15.91) | -13.03 (-23.06, -3.00) |
| Fast BKMR | <i>h</i> (NO ₂ , CO, PM _{2.5}) | -18.18 (-24.87, -11.48) | -16.24 (-26.08, -6.41) |

models, the birthweight reduction from the exposure contrast of 95th to 50th percentiles were consistently smaller than that from the exposure contrast of 75th to 25th percentiles. However, unlike the linear models, Fast BKMR showed similar birthweight reductions for both exposure contrasts. Regardless of the exposure contrast, the single pollutant model consistently estimated smaller reduction in birthweight associated with air pollution. For the exposure contrast between 75th and 25th percentiles, multi-pollutant models with interaction terms had the largest effect sizes, with birthweight reductions reaching up to 25.06 grams (95% confidence interval (CI): 15.91, 34.21). For Fast BKMR, the reduction in birthweight was 18.18 (95% posterior interval (PI): 11.48, 24.87) grams, which is smaller than the effects size from multi-pollutant model but with a narrower 95% PI. The difference in birthweight reduction between multi-pollutant models and Fast BKMR can be caused by the collinearity among exposures and different ways that exposure effects are aggregated. For the exposure contrast between 95th and 50th percentiles, the birthweight reduction from Fast BKMR was 16.24 grams (95% PI: 6.41, 26.08), while multi-pollutant models estimated a smaller reduction in birthweight.

Figure 2 shows the overall effects of all three pollutants on birthweight differences, setting all three pollutants to their 25th percentiles as the reference level. As the percentiles of the

pollutants increased, birthweight initially increased slightly, followed by a large decrease. When three pollutants were at their 50th percentiles, the reduction in average birthweight was around 7 grams. When all pollutants further increased to 95th percentiles, the reduction exceeded 20 grams. The blue-shaded areas represent the 95% posterior intervals. If the shaded region does not overlap with zero, it indicates a significant reduction in birthweight. We observed a significant reduction in birthweight when all exposures exceeded the 50th percentile compared to when all exposures were at the 25th percentile.

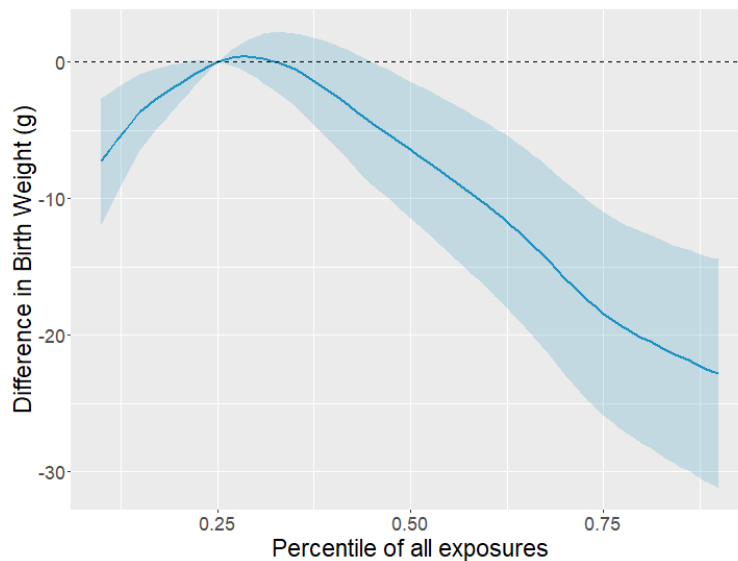


Figure 2: The overall effects of all exposures on the birthweight compared to the 25th percentiles of exposures with 20 basis functions. Blue-shaded areas are the 95% posterior intervals.

To explore the single pollutant effects, we constructed univariate exposure-response functions for each single pollutant while fixing the other two pollutants at 10th, 50th and 90th percentiles. The possible range of each single pollutant was determined by varying the other two pollutants between the $(P - 5)^{th}$ and $(P + 5)^{th}$ percentiles, where P represents the fixed percentiles of the two pollutants. For example, when we fixed CO and NO₂ at their 10th percentiles, we generated response function for the observed range of PM_{2.5} concentrations where CO and NO₂ were between their 5th and 15th percentiles.

As shown in Figure 3, we found that increasing PM_{2.5} was significantly associated with

decreasing birthweight when CO and NO₂ were fixed at their 50th and 90th percentiles. For NO₂, we also observed birthweight reduction with increasing NO₂ levels when the other two pollutants were fixed at 50th and 90th percentiles, although this reduction had larger posterior intervals. In contrast, a reverse association was observed for CO, where birthweight increased with higher CO levels, regardless of the percentiles at which the other two pollutants were fixed.

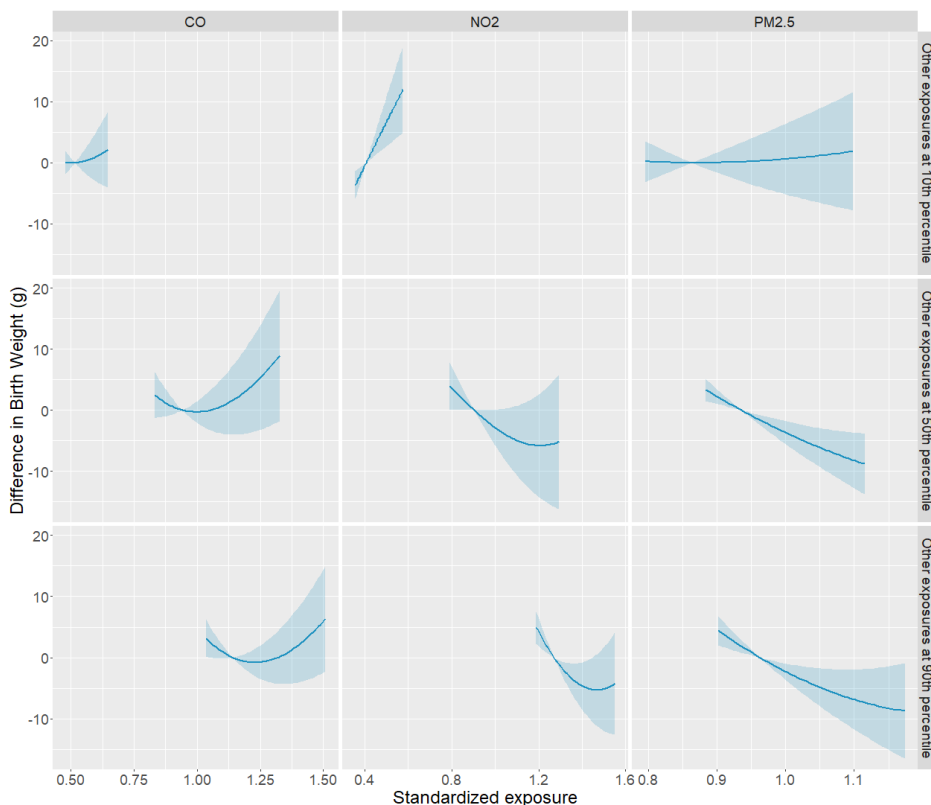


Figure 3: The response plots for single pollutant when fixing other two pollutants at 10th, 50th and 90th percentiles.

Finally, we explored the joint effects between two pollutants, fixing the third pollutant at its 50th percentiles. The difference in birthweight was compared to the birthweight level when both two pollutants were at their 25th percentiles. As shown in Figure 4 A, the bi-pollutant exposure-response surface indicated that birthweight decreased as NO₂ and PM_{2.5} concentrations increased together. The reduction in birthweight exceeded 20 grams when standardized PM_{2.5} was over 1.1 and NO₂ around 1.2. When PM_{2.5} was fixed at specific

concentration, birthweight reduced with increasing NO_2 , except when $\text{PM}_{2.5}$ concentration is also low. When standardized NO_2 was above 0.8, increasing $\text{PM}_{2.5}$ was consistently associated with a reduced birthweight. To make the bi-pollutant exposure-response surface more accessible, we present bi-pollutant exposure-response functions for pairwise exposures, where the second exposure is fixed at the 25th, 50th, and 75th percentiles, in Figures 4 B and C. The estimated difference in birthweight in Figures 4 B and C is the same as the values represented by dashed lines in Figures 4 A, but we also provide the 95% posterior intervals for inference. As shown in Figure 4 B, increasing $\text{PM}_{2.5}$ is associated with a greater reduction in birthweight at higher percentiles of NO_2 . This reduction is significant when standardized $\text{PM}_{2.5}$ exceeds 1.05, with NO_2 fixed at the 50th and 75th percentiles. In Figure 4 C, we observe a similar pattern, where a greater reduction in birthweight is associated with higher percentiles of $\text{PM}_{2.5}$ and increasing NO_2 levels between 0.8 and 1.2. This reduction is significant when NO_2 is fixed at the 75th percentile. The bi-pollutant exposure-response surfaces for standardized CO and $\text{PM}_{2.5}$ and for standardized CO and NO_2 are shown in Web Figures 3 and 4, respectively.

5 Discussion

In this study, we used supervised RFF to approximate Gaussian process, addressing the issue of computation time for BKMR with large datasets. According to the simulation studies, our approximation methods can reduce computation time of the original BKMR by 29 to 99%, depending on the number of basis functions. Even if we employed the Gaussian predictive process to speed up model fitting in the original BKMR, our approximation approach is able to reduce 88% computation time when we compared 50 knots and 50 basis functions for 1000 observations and 5 exposures. Additionally, when sample size is small where the original BKMR is feasible, our approximation may also improve the estimation, particularly when the kernel induces strong correlation, which is commonly observed among

air pollutants . In scenarios with incorrect kernel specification, our proposed method is still able to capture the exposure-response relationships and out-performs BKMR when exposures are strongly correlated, and their number is large. Our approach can also estimate marginal, single- and two-exposure exposure-response functions much faster than BKMR because matrix inversion is not needed in prediction.

Our findings on the effects of individual pollutants on birthweight, while holding the other two exposures constant, align with previous literature, showing that both NO_2 and $\text{PM}_{2.5}$ are associated with a reduction in birthweight (Strickland et al., 2019; Li et al., 2019; Bekkar et al., 2020). According to the univariate exposure-response plots, we found positive association between CO and birthweight but this association is not statistically significant. To our knowledge, this is the first large-scale analysis of joint air pollutant effects on birthweight from administrative data using BKMR, offering new insights into the nonlinear and joint effects of air pollutants. In addition to using 20 basis functions, we also examined 5 and 50 basis functions. The overall and single exposure-response plots using 50 basis functions showed associations very similar to those observed with 20 basis functions. The exposure-response plots with 5 basis functions appeared closer to a straight line, indicating few basis functions may not be enough. The selection of the number of basis functions depends on various factors, including the number of exposures, sample size, and correlations between exposures. It is advisable to begin with a small number of basis functions and evaluate different choices to determine the optimal number.

Another advantage of using an approximation method is the ability to handle highly correlated random effects. In Gaussian process regression, the kernel matrix can become numerical singular (Kanagawa et al., 2018). This issue is common in environmental health studies on air pollution, where people living in the same areas, such as Census tracts or ZIP codes, often share the same exposure information, making them perfectly or highly correlated. By avoiding the inversion of the kernel matrix in our approximation approach, we eliminate this issue.

One extension of our proposed method is to consider variable selection. Specifically, stochastic variable selection can be conducted to exclude exposures from contributing to the kernel function. In the similar linear mixed-effect model framework, this is accomplished by placing a spike-and-slab prior on kernel parameter θ_m around zero (Ishwaran and Rao, 2005; Chen and Dunson, 2003). The current implementation of BKMR allows for variable selection, offering an approach for dimension reduction (Bobb et al., 2014). BKMR introduced variable selection to deal with highly correlated exposures while our approximation method handles highly correlated exposures by learning the optimal frequencies for a small number of basis functions. Moreover, in population-based health studies examining the effects of multiple air pollutants or the effects of chemicals with extensive biomonitoring, the number of exposures is typically much smaller than the sample size. Hence, dimensionality reduction is not always needed to characterize the exposure-response function.

There are other further methodological investigations for the Fast BKMR. First, compared with non-Bayesian methods, such as WQS and q-gcomp, the Fast BKMR is still time consuming. Since BKMR is preferred in scenarios considering non-linear effects and interactions, we may consider approaches to improve the computation of BKMR without MCMC. Second, our current method only works for continuous outcomes. One potential extension is to apply this approximation method in a generalized linear model framework, where the outcome can follow Binomial or Poisson distributions.

6 Acknowledgements

This work was supported by grants from the National Institute of Environmental Health Sciences under Award Numbers R01ES028346 and K01ES035082. Any opinions, findings, and conclusions or recommendations expressed in this material are those of the authors and do not necessarily reflect the views of the funders.

References

- Banerjee, S., Gelfand, A. E., Finley, A. O., and Sang, H. (2008). Gaussian predictive process models for large spatial data sets. *Journal of the Royal Statistical Society: Series B (Statistical Methodology)*, 70(4):825–848.
- Banerjee, S. (2017). High-dimensional Bayesian geostatistics. *Bayesian Analysis*, 12(2):583–614.
- Bekkar, B., Pacheco, S., Basu, R., and DeNicola, N. (2020). Association of air pollution and heat exposure with preterm birth, low birth weight, and stillbirth in the us: A systematic review. *JAMA Network Open*, 3(6):e208243–e208243.
- Benka-Coker, W., Hoskovec, L., Severson, R., Balmes, J., Wilson, A., and Magzamen, S. (2020). The joint effect of ambient air pollution and agricultural pesticide exposures on lung function among children with asthma. *Environmental Research* **190**, 109903.
- Billionnet, C., Sherrill, D., and Annesi-Maesano, I. (2012). Estimating the health effects of exposure to multi-pollutant mixture. *Annals of Epidemiology* **22**, 126–141.
- Bobb, J. F., Valeri, L., Claus Henn, B., Christiani, D. C., Wright, R. O., Mazumdar, M., Godleski, J. J., and Coull, B. A. (2014). Bayesian kernel machine regression for estimating the health effects of multi-pollutant mixtures. *Biostatistics* **16**, 493–508.
- Bobb, J. F., Claus Henn, B., Valeri, L., and Coull, B. A. (2018). Statistical software for analyzing the health effects of multiple concurrent exposures via Bayesian kernel machine regression. *Environmental Health: A Global Access Science Source*, 17(1), 67.
- Bobb, J. F. (2022). Bayesian Kernel Machine Regression. *R package version 0.2.2*. Available at <https://CRAN.R-project.org/package=bkmr>.

- Chang, W.-C., Li, C.-L., Yang, Y., and Póczos, B. (2017). Data-driven random fourier features using stein effect. *arXiv preprint arXiv:1705.08525*.
- Chen, Z. and Dunson, D. B. (2003). Random effects selection in linear mixed models. *Biometrics*, 59(4):762–769.
- Eick, S. M., Tan, Y., Taibl, K. R., Ryan, P. B., Barr, D. B., Hüls, A., Eatman, J. A., Panuwet, P., D’Souza, P. E., Yakimavets, V., et al. (2024). Prenatal exposure to persistent and non-persistent chemical mixtures and associations with adverse birth outcomes in the atlanta african american maternal-child cohort. *Journal of exposure science & environmental epidemiology*, 34(4):570–580.
- Finley, A. O., Sang, H., Banerjee, S., and Gelfand, A. E. (2009). Improving the performance of predictive process modeling for large datasets. *Computational Statistics & Data Analysis*, 53(8):2873–2884.
- Friberg, M. D., Zhai, X., Holmes, H. A., Chang, H. H., Strickland, M. J., Sarnat, S. E., Tolbert, P. E., Russell, A. G., and Mulholland, J. A. (2016). Method for fusing observational data and chemical transport model simulations to estimate spatiotemporally resolved ambient air pollution. *Environmental Science & Technology* **50**, 3695–3705. PMID: 26923334.
- Gelman, A., Carlin, J., Stern, H., Dunson, D., Vehtari, A., and Rubin, D. (2013). *Bayesian Data Analysis, Third Edition*. Chapman & Hall/CRC Texts in Statistical Science. Taylor & Francis.
- Ishwaran, H. and Rao, J. S. (2005). Spike and slab variable selection: Frequentist and Bayesian strategies. *The Annals of Statistics* **33**, 730 – 773.
- Kanagawa, M., Hennig, P., Sejdinovic, D., and Sriperumbudur, B. K. (2018). Gaussian processes and kernel methods: A review on connections and equivalences. *arXiv preprint arXiv:1807.02582* .

- Kim, C., Kim, B., Kim, S., and Park, B. (2024). Association between long-term exposure to mixture of ambient air pollutants and bladder cancer incidence. In *ISEE Conference Abstracts*, volume 2024.
- Kishore Kumar, N. and Schneider, J. (2017). Literature survey on low rank approximation of matrices. *Linear and Multilinear Algebra* **65**, 2212–2244.
- Li, Z., Yuan, X., Fu, J., Zhang, L., Hong, L., Hu, L., and Liu, L. (2019). Association of ambient air pollutants and birth weight in ningbo, 2015–2017. *Environmental Pollution*, 249:629–637.
- Li, H., Deng, W., Small, R., Schwartz, J., Liu, J., and Shi, L. (2022). Health effects of air pollutant mixtures on overall mortality among the elderly population using bayesian kernel machine regression (bkmr). *Chemosphere* **286**, 131566.
- Liu, F., Huang, X., Chen, Y., and Suykens, J. A. (2021). Random features for kernel approximation: A survey on algorithms, theory, and beyond. *IEEE Transactions on Pattern Analysis and Machine Intelligence* **44**, 7128–7148.
- Miller, M. J. and Reich, B. J. (2022). Bayesian spatial modeling using random fourier frequencies. *Spatial Statistics* **48**, 100598.
- Neal, R. (2011). Handbook of markov chain monte carlo, volume 2, chapter mcmc using hamiltonian dynamics.
- Preston, E. V., Webster, T.F., Henn, B. C., McClean, M. D., Gennings, C., Oken, E., Rifas-Shiman, S. L., Pearce, E. N., Calafat, A. M., Fleisch, A. F., et al. (2020). Prenatal exposure to per-and polyfluoroalkyl substances and maternal and neonatal thyroid function in the project viva cohort: A mixtures approach. *Environment international*, 139:105728.
- R Core Team (2022). *R: A Language and Environment for Statistical Computing*. R Foundation for Statistical Computing, Vienna, Austria.

- Rahimi, A. and Recht, B. (2007). Random features for large-scale kernel machines. *Advances in neural information processing systems* **20**,
- Rudin, W. (2017). *Fourier analysis on groups*. Courier Dover Publications.
- Sexton, K. (2012). Cumulative risk assessment: an overview of methodological approaches for evaluating combined health effects from exposure to multiple environmental stressors. *International journal of environmental research and public health* **9**, 370–390.
- Shiroshita, A., Kataoka, Y., Wang, Q., Kajita, N., Anan, K., Tajima, T., and Yajima, N. (2024). Joint associations of air pollutants during pregnancy, infancy, and childhood with childhood persistent asthma: Nationwide database study in japan. *Ecotoxicology and Environmental Safety* **281**, 116626.
- Strickland, M. J., Lin, Y., Darrow, L. A., Warren, J. L., Mulholland, J. A., and Chang, H. H. (2019). Associations between ambient air pollutant concentrations and birth weight: a quantile regression analysis. *Epidemiology* **30**, 624–632.
- Yang, X., Li, Y., Li, J., Bao, S., Zhou, A., Xu, S., and Xia, W. (2020). Associations between exposure to metal mixtures and birth weight. *Environmental Pollution* **263**, 114537.
- Zhuang, L. H., Chen, A., Braun, J. M., Lanphear, B. P., Hu, J. M., Yolton, K., and McCandless, L. C. (2021). Effects of gestational exposures to chemical mixtures on birth weight using bayesian factor analysis in the health outcome and measures of environment (home) study. *Environmental Epidemiology* **5**, e159.

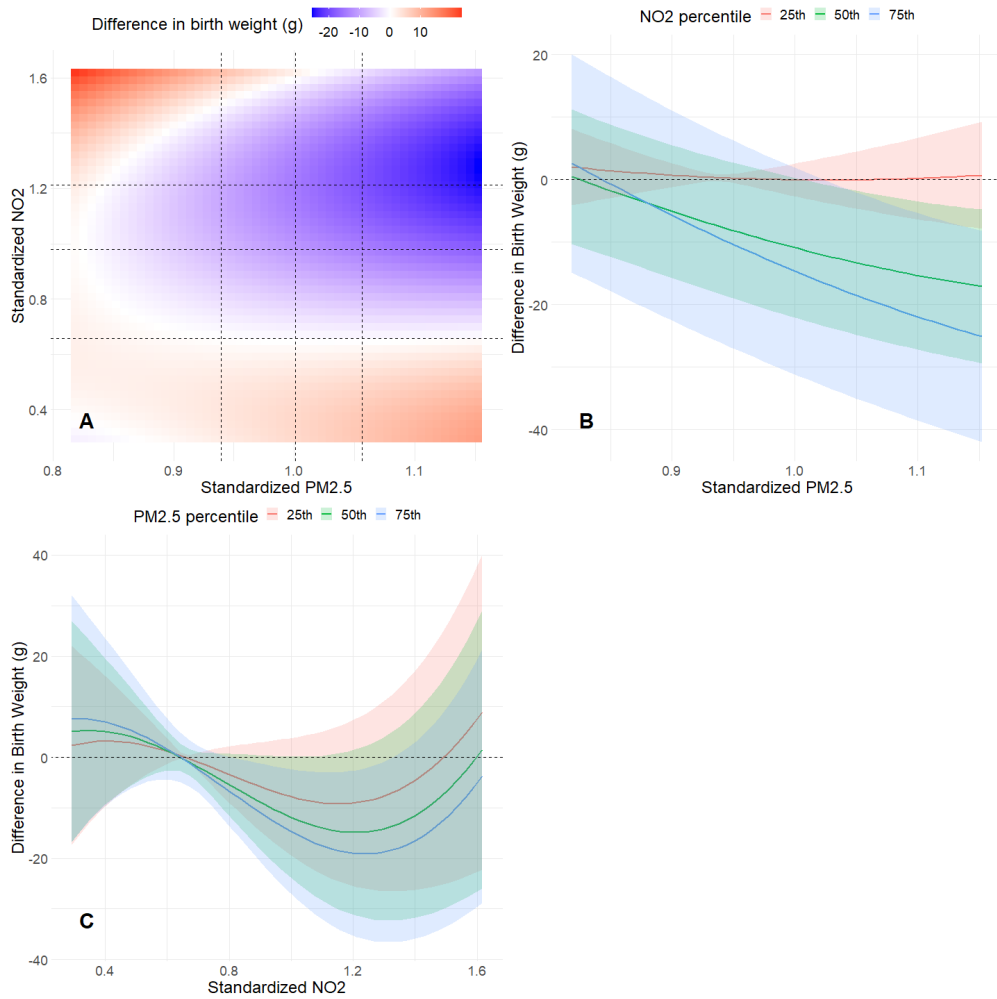


Figure 4: **A.** Bi-pollutant exposure-response surface for standardized PM_{2.5} and NO₂ when fixing the CO at 50th percentiles. Vertical dashed lines are 25th, 50th and 75th percentiles of standardized PM_{2.5} (from left to right). Horizontal dashed lines are 25th, 50th and 75th percentiles of standardized NO₂ (from bottom to top). **B.** Bi-pollutant exposure-response functions for standardized PM_{2.5} at 25th, 50th and 75th percentiles of the NO₂, with CO fixed at 50th percentiles. **C.** Bi-pollutant exposure-response functions of standardized NO₂ with 25th, 50th and 75th percentiles of the PM_{2.5} with CO fixed at 50th percentiles.

Supplementary Materials for “Approximate Bayesian Kernel
Machine Regression via Random Fourier Features for Estimating
Joint Health Effects of Multiple Exposures” by Danlu Zhang,
Stephanie M. Eick, and Howard H. Chang

Web Appendix A Hamiltonian Monte Carlo (HMC) updates

For regression coefficients $\Theta = (\gamma_1, \dots, \gamma_P, a_1, \dots, a_J, b_1, \dots, b_J)^T$ updates, let \mathbf{B} be the $n \times (P + 2J)$ design matrix with each row having elements

$$[Z_{i1}, \dots, Z_{iP}, \cos(\boldsymbol{\omega}_1^T \mathbf{x}_i), \dots, \cos(\boldsymbol{\omega}_J^T \mathbf{x}_i), \sin(\boldsymbol{\omega}_1^T \mathbf{x}_i), \dots, \sin(\boldsymbol{\omega}_J^T \mathbf{x}_i)]$$

Then $\mathcal{L}(\Theta)$ and $\nabla \mathcal{L}(\Theta)$ used in HMC is

$$\mathcal{L}(\Theta) = -\frac{1}{2\sigma^2}(\mathbf{Y} - \mathbf{B}\Theta)^T(\mathbf{Y} - \mathbf{B}\Theta) - \frac{1}{2}\Theta^T \mathbf{S}^{-1}\Theta$$

and

$$\nabla_{\Theta} \mathcal{L}(\Theta) = \frac{1}{\sigma^2} \mathbf{B}^T (\mathbf{Y} - \mathbf{B}\Theta) - \mathbf{S}^{-1}\Theta$$

where $\mathbf{S} = \text{diag}(\sigma_{\gamma}^2, \dots, \sigma_{\gamma}^2, \tau^2/J, \dots, \tau^2/J)$.

For $\boldsymbol{\omega}_j$ updates, let \mathbf{B}_{cos} be the design matrix with rows $[\cos(\boldsymbol{\omega}_1^T \mathbf{x}_i), \dots, \cos(\boldsymbol{\omega}_J^T \mathbf{x}_i)]$, and similarly define \mathbf{B}_{sin} . Then

$$\mathcal{L}(\Omega) = -\frac{1}{2\sigma^2} \|\mathbf{Y} - \mathbf{B}_{cos} \mathbf{a} - \mathbf{B}_{sin} \mathbf{b} - \mathbf{Z}^T \boldsymbol{\gamma}\|^2 - \frac{1}{2} \sum_{j=1}^J \boldsymbol{\omega}_j^T \boldsymbol{\Sigma}^{-1} \boldsymbol{\omega}_j$$

$$\nabla_{\Omega} \mathcal{L}(\Omega)_{J \times M} = -\frac{1}{\sigma^2} \mathbf{D}^T (\mathbf{X} \odot [\mathbf{R} \mid \dots \mid \mathbf{R}]) - \Omega^*$$

where \odot is the Hadamard (element-wise) product, and

$$\mathbf{D} = \mathbf{B}_{sin} \odot [\mathbf{a} \mid \mathbf{a} \mid \dots \mid \mathbf{a}]^T - \mathbf{B}_{cos} \odot [\mathbf{b} \mid \mathbf{b} \mid \dots \mid \mathbf{b}]^T$$

$$\mathbf{R} = \mathbf{Y} - \mathbf{B}_{cos} \mathbf{a} - \mathbf{B}_{sin} \mathbf{b} - \mathbf{Z} \boldsymbol{\gamma}$$

$$\Omega^* = [\boldsymbol{\Sigma}^{-1} \boldsymbol{\omega}_1 \mid \boldsymbol{\Sigma}^{-1} \boldsymbol{\omega}_2 \mid \dots \mid \boldsymbol{\Sigma}^{-1} \boldsymbol{\omega}_J]^T$$

Web Appendix B R code for implementing Fast BKMR

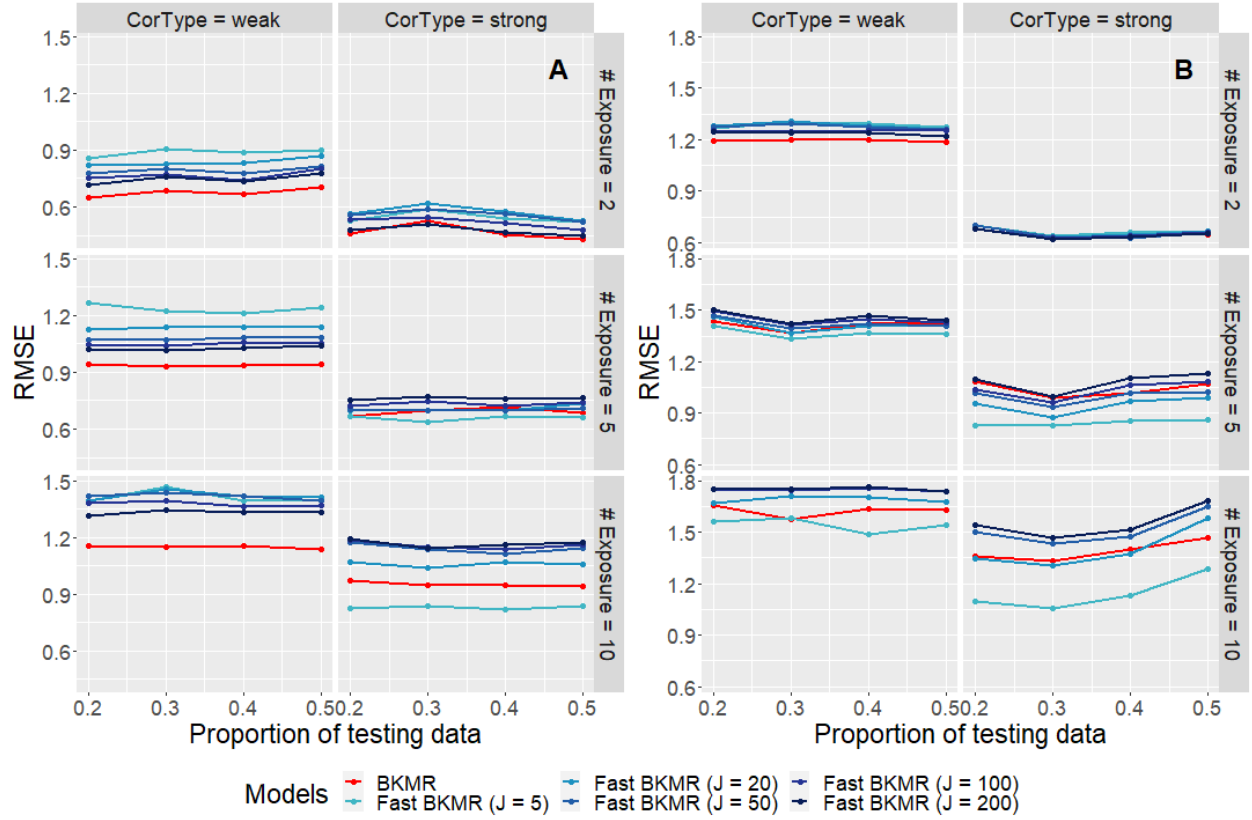
R code used to implement the proposed methods is available at
https://github.com/Danlu233/Fast_BKMR.git

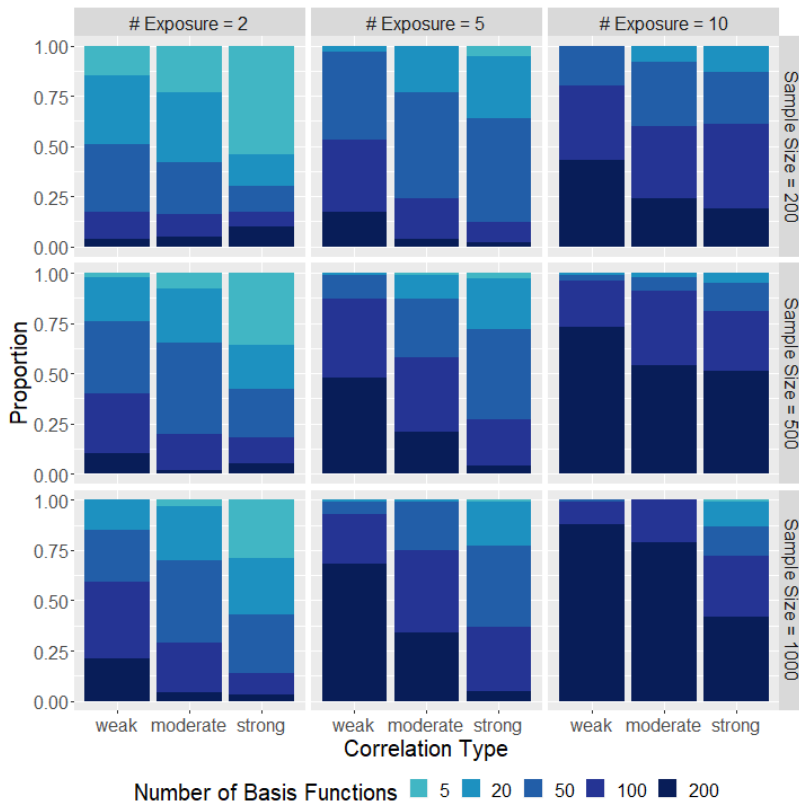
Web Table 1: Population Characteristics in Atlanta Birthweight Study.

| Characteristics | Overall (N = 273,711) |
|--|-----------------------|
| Maternal race/ethnicity | |
| White | 121,056 (44.2%) |
| Black | 84,193 (30.8%) |
| Asian | 13,114 (4.8%) |
| Hispanic | 53,831 (19.7%) |
| Other | 1,517 (0.6%) |
| Maternal age | |
| 16 - 25 years | 89,401 (32.7%) |
| 25 - 31 years | 104,352 (38.1%) |
| 31 - 43 years | 79,958 (29.2%) |
| Maternal education | |
| Less than 9th grade | 22,656 (8.3%) |
| 9th-12th grade | 39,236 (14.3%) |
| High School | 76,481 (27.9%) |
| College and above | 135,338 (49.4%) |
| Maternal tobacco use | 12,644 (4.6%) |
| Maternal alcohol use | 1,723 (0.6%) |
| Maternal married | 174,009 (63.6%) |
| Previous birth | 164,202 (60.0%) |
| Gestational weeks | |
| Mean (SD) | 38.7 (1.8) |
| [Min, Max] | [28.0, 44.0] |
| Census block group percent poverty levels | |
| Mean (SD) | 0.10 (0.10) |
| [Min, Max] | [0, 0.77] |

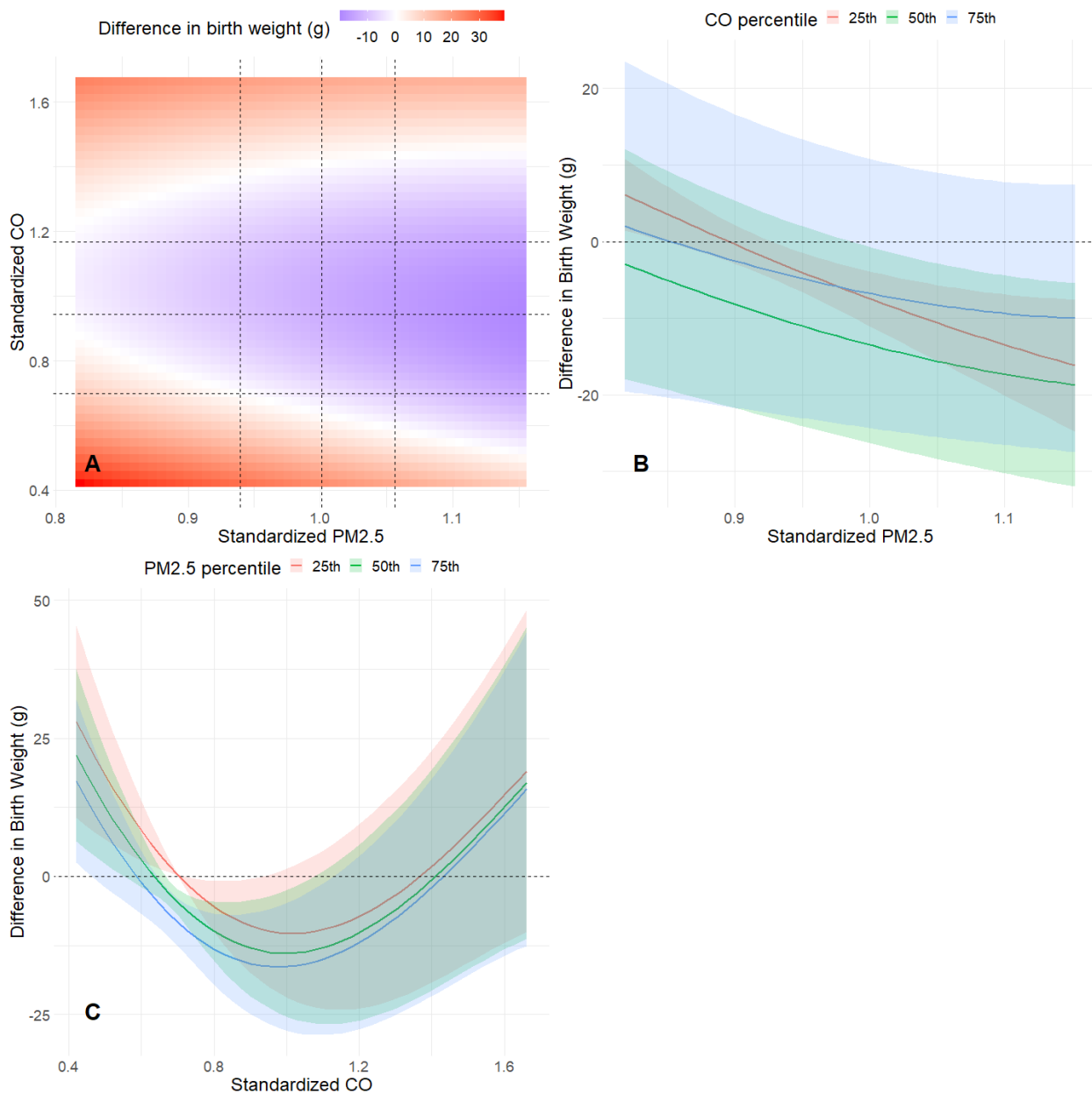
Web Table 2: Statistics Summary of Pollutants in Atlanta Birthweight Study (original scale).

| Pollutant | Mean (SD) | [Min, Max] | IQR |
|--|--------------|----------------|-------|
| NO ₂ (ppb) | 22.03 (7.86) | [3.88, 40.47] | 12.96 |
| CO (ppm) | 0.70 (0.23) | [0.23, 1.41] | 0.34 |
| PM _{2.5} (μg/m ³) | 15.90 (1.24) | [11.19, 20.66] | 1.86 |

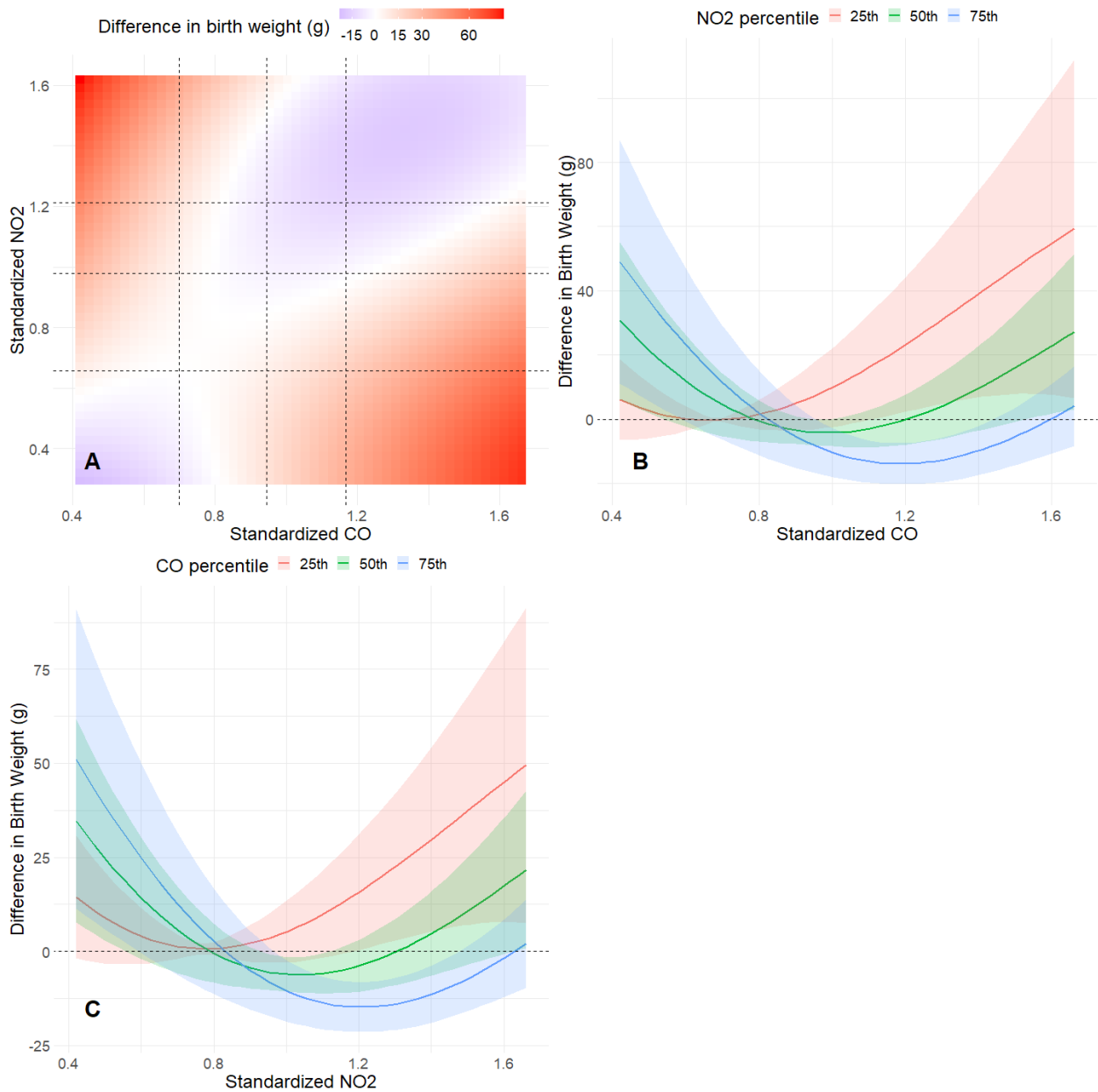




Web Figure 2: The proportion of selected number of basis functions based on WAIC.



Web Figure 3: **A.** Bi-pollutant exposure-response surface for standardized CO and PM_{2.5} when fixing the NO₂ at 50th percentiles. Vertical dashed lines are 25th, 50th and 75th percentiles of standardized PM_{2.5} (from left to right). Horizontal dashed lines are 25th, 50th and 75th percentiles of standardized CO (from bottom to top). **B.** Bi-pollutant exposure-response functions for standardized PM_{2.5} at 25th, 50th and 75th percentiles of the CO, with NO₂ fixed at 50th percentiles. **C.** Bi-pollutant exposure-response functions of standardized CO with 25th, 50th and 75th percentiles of the PM_{2.5} with NO₂ fixed at 50th percentiles.



Web Figure 4: **A.** Bi-pollutant exposure-response surface for standardized CO and NO₂ when fixing the PM_{2.5} at 50th percentiles. Vertical dashed lines are 25th, 50th and 75th percentiles of standardized CO (from left to right). Horizontal dashed lines are 25th, 50th and 75th percentiles of standardized NO₂ (from bottom to top). **B.** Bi-pollutant exposure-response functions for standardized CO at 25th, 50th and 75th percentiles of the NO₂, with PM_{2.5} fixed at 50th percentiles. **C.** Bi-pollutant exposure-response functions of standardized NO₂ with 25th, 50th and 75th percentiles of the CO with PM_{2.5} fixed at 50th percentiles.